Effect of processing on microstructure, mechanical properties and dissolution behaviour in SBF of Bioglass (45S5) coatings deposited by Suspension High Velocity Oxy Fuel (SHVOF) thermal spray

S. Bano, I. Ahmed, D.M. Grant, A. Nommeots-Nomm, T. Hussain

PII: S0257-8972(19)30518-3
DOI: https://doi.org/10.1016/j.surfcoat.2019.05.038
Reference: SCT 24627

To appear in: *Surface & Coatings Technology*

Received date: 1 March 2019
Revised date: 7 May 2019
Accepted date: 12 May 2019

Please cite this article as: S. Bano, I. Ahmed, D.M. Grant, et al., Effect of processing on microstructure, mechanical properties and dissolution behaviour in SBF of Bioglass (45S5) coatings deposited by Suspension High Velocity Oxy Fuel (SHVOF) thermal spray, Surface & Coatings Technology, https://doi.org/10.1016/j.surfcoat.2019.05.038

Effect of processing on microstructure, mechanical properties and dissolution behaviour in SBF of Bioglass (45S5) coatings deposited by Suspension High Velocity Oxy Fuel (SHVOF) thermal spray

S. Bano[1], I. Ahmed[1], D. M. Grant[1], A. Nommeots-Nomm[2], T. Hussain[1]

Faculty of Engineering, Advanced Materials Research Group, University of Nottingham, NG7 2RD, UK[1]

Department of Mining and Materials Engineering, McGill University, 3610 University Street, Wong Building, Montreal, Quebec, H3A 0C5, Canada[2]

Abstract: Bioglass (45S5) is known to react with physiological media and has the unique characteristic of bonding with hard and soft tissues when implanted in the body. 45S5 coatings were deposited by suspension high velocity oxy fuel (SHVOF) thermal spraying to investigate the effect of combustion conditions on the coating microstructure and surface topography. Bioactive (45S5) coatings were deposited onto 304 stainless steel substrates via SHVOF thermal spray using a water + isopropanol (IPA) based suspension with 8 wt. % particle loading. Selected flame powers of 25 kW (low), 50 kW (medium) and 75 kW (high) produced three different coatings of varying microstructure (porosity and thickness) and composition. At 25 kW flame power thin coating of <10 µm thickness was deposited; however, 25 ± 3 µm thick, well bonded coatings to the substrates were deposited at flame powers of 50 and 75 kW. The medium flame power coating was 16±2 % porous, while the high flame power coating was 10 ± 1 % porous. All the coatings remained amorphous, as confirmed via X-ray diffraction. After immersing the coated samples in simulated body fluid (SBF), 50 and 75 kW coatings revealed hydroxyapatite (HA) deposition after 3 days. Also, no HA deposition was observed on 25 kW coating, even after 7 days of immersion in SBF. EDX analysis of the 50 kW coating after 7 days immersion in SBF showed that the initial coating thickness reduced from 25 µm to 6 µm, it means that this microstructure was highly reactive towards SBF and hence behaved like a resorbable coating. Through SHVOF

spraying technique changing the flame power resulted in coatings of varying microstructure. These microstructures behaved differently in SBF, 50 kW coating showed more degradation than the 75 kW coating owing to the porosity.

Keywords: SHVOF, thermal spray, 45S5, Bioglass, Hydroxyapatite (HA), simulated body fluid (SBF)

1 Introduction

Bioglass (45S5) is a soda lime phosphosilicate glass (Na_2O-CaO-P_2O-SiO_2) which is known to react with physiological media and has the unique characteristic of bonding with hard and soft tissues when implanted in the body [1]–[4]. The proposed mechanism for bond formation with the host tissue involves partial dissolution by the body fluid releasing calcium and phosphate ions which increase local pH and also Si-(OH) group forms. The Si-(OH) groups polymerise on the surface of the Bioglass and produce a porous silica gel film tens of microns thick on the glass surface via hydrolysis [5]. On the surface of this silica layer hydroxyl-carbonate apatite (HCA) nucleates and grows. The dissolution products of Bioglass (45S5) stimulate progenitor cells to differentiate a bone cell and the process of osteoindustion starts [1][6]. It has also been suggested that the release of Si ions (as a result of degradation) can stimulate cellular activity which promotes bone formation and bonding of the new tissue on the surface of Bioglass [7], making these glasses osteoconductive, which causes bone formation at the surface of the implant. Also Bioglass (45S5) is osteointegrative which means that the implant makes bond with the host tissue[7]–[9].

However, Bioglass and other bioactive glasses are brittle and have poor fracture toughness (0.6 MPa $m^{1/2}$) and tensile strength (42 MPa) making them unsuitable for structural purposes, where metallic alloys are still the materials of choice to use as bone implants [8][10]. One option is to apply the Bioglass as a coating on metallic implants to enable the component to be bioactive [9]. While the substrate provides the mechanical load bearing capabilities the Bioglass contributes to the bioactivity of the implant surface [11]. A

bioactive coating needs to have a good adhesion to the substrate, and avoid degradation of the feedstock powder during deposition. Different methods have been applied for the production of Bioglass (45S5) and bioactive glass coatings such as sol–gel processing, laser processing, dip-coating, electrophoretic deposition, physical vapour deposition, air brush spraying and plasma spray [12]. Among them the innovative technique of SHVOF thermal spray made it possible to process sub micron and nano glass particles and produce dense, well adherent coatings [13]–[14]. Moreover with SHVOF thermal spray relatively thicker coating can be deposited [11], which is good for bioactive coatings. Because it has been shown that if the bioactive glass coating is thin, the reactions between the coating and surrounding media may involve the whole coating which is detrimental for its adhesion with the substrate [15] . By SHVOF thermal spray compact glass coatings with excellent mechanical properties has been deposited [16] and has been proven to be a viable technique for depositing hydroxyapatite (HA) and bioactive glass coatings as well [17]–[20].

There are large number of processing parameters in SHVOF thermal spraying, and this study aimed to investigate how these processing parameters, especially combustion characteristics, can influence Bioglass (45S5) coatings microstructure and phase compositions. To our knowledge, a detailed investigation on the role of flame powers on the microstructure of a Bioglass has never been reported. The novelty of the study lies in developing three distinctly different microstructure of 45S5 Bioglass from three different combustion flame powers. The microstructure of the SHVOF deposited Bioglass (45S5) coatings was examined by scanning electron microscopy (SEM), microhardness and surface profilometry. Phase identification was performed using X-ray diffraction (XRD) and Raman spectroscopy. The coatings bioactivity was explored by soaking coated materials in simulated body fluid (SBF). A mechanism of degradation in SBF was proposed in relation to different coatings microstructure.

2 Experimental methods

2.1 Powder and Suspension preparation

45S5 Bioglass with chemical composition (46.1 SiO_2, 26.9 CaO, 24.4 Na_2O, and 2.6 P_2O_5- all in mol. %) was used for this study. 45S5 was produced via a melt quenching process. Carbonate equivalents of modifying oxides, phosphorus pentoxide with 99% purity (Sigma Aldrich UK), and high purity (99.5%) silica (High Purity, Prince Minerals, Stoke-on-Trent), were weighed and mixed for 8 h using a Wheaton mini roller, UK. The powder was then melted at 1400 °C for 2 h, in a 95% platinum 5% gold crucible. The melt was then quenched in deionized water. The formed frit was then collected and dried at 100°C, and then dry milled using a zirconia jar with zirconia balls of 5 mm diameter for 30 min and 550 rpm using PM-100 ball mill (Retsch1-5, Germany), resulting in D_{10}= 2 µm, D_{50}= 21 µm and D_{90}= 55 µm for the powders. The resulting powder was again dry milled with zirconia beads of 2 mm diameter for 30 minutes at 500 rpm, while the ball to particle weight ratio was approximately 5. Particle size distribution (D_{10}, D_{50}, and D_{90}) was measured by laser diffraction (Beckman Coulter, Inc., 250 S.Kraemer Blvd. Brea, (California 92821, USA) using a 750 nm laser.

Liquid suspension was prepared in a mixed solvent of water and alcohol, to prevent leaching out of alkali and alkaline metallic oxides form 45S5. 45S5 suspension was made by dispersing 8 wt.% of 45S5 to 92 wt.% of liquid phase consisting of 85 wt.% of water and 15 wt.% of isopropyl alcohol (IPA)[21][22].

2.2 Coating Deposition

The 304 Stainless steel substrates (nominal composition of 9.25 Ni, 19.0 Cr, 1.0 Si, 2.0 Mn, 0.08 C, 0.04 P, 0.03 S and 68.6 Fe—all in wt. %) (60 x 25 x 2 mm) were grit blasted (Guyson blast cleaner, England) with F100 brown alumina (0.125-0.149 mm) particles at 3 bar and cleansed in industrial methylated spirit (IMS) in an ultrasonic bath for up to 10 min,

followed by drying with compressed air. The substrates were then mounted onto a rotating carousel (73 rpm) of twelve substrate holders whilst the spray gun moved orthogonally to the substrates at a speed of 5 mm/s.

The SHVOF system has already been fully described in [23]. In brief, coatings were fabricated using modified UTP Top Gun HVOF thermal spray unit (Miller Thermal Inc., USA) with axial injection of liquid suspension from a 0.3 mm nozzle delivered from a 2 L pressurized vessel at pressure of 3 bar with a flow rate of 80 ml/min on substrates. The length of the combustion chamber was 22 mm with 110 mm long barrel nozzle. The coatings were cooled with pressurized air during deposition and after spray. Flow rates of fuel gas (Hydrogen) and oxygen were set by using a volume control system as given in Table 1. Different spray runs were made by changing these flow rates whilst other parameters such as suspension flow rate (50 ml/min) spray distance (85 mm), and torch passes (20) were kept constant. Theoretical flame heat power for each run was calculated using standard combustion formulas.

2.3 Characterisation of the coatings

The glass powder was characterised by scanning electron microscope (SEM, Quanta-600) at 20 kV, whilst the size distribution of the particles for both steps of ball milling was measured by laser diffraction Beckman Coulter, Inc.250 S. Kraemer Blvd. Brea, (California 92821, USA). Coated samples were cut transversely, hot mounted in conductive resin (Bakelite) and polished to 1 µm diamond finish.

Quanta-600 SEM was used to examine the coating microstructure under secondary electron (SE) mode. EDX line scan along the cross-section of coatings was done using SEM (JEOL 6490, Tokyo Japan, EDX: INCA 350, Oxford Instruments, Abingdon, UK). Surface roughness of the coatings was measured using white light sourced Zygo NewView 8300 [37]

with 5.5× objective at 0.5× zoom (NA 0.15, field of view (3.02 × 3.02) mm, LR-pixel 2.95 µm, LR-optical 1.82 µm), where LR is lateral resolution. Measurement of five fields of view per sample, located at various positions across the sample (using Zygo proprietary software) was made. The porosity of each coating was analysed from five SEM (SE) images (270 µm× 232 µm) using thresholding technique in image-J software ((NIH, USA). Coating thickness was measured with the same software at five different locations by using SEM images (134× 117µm) of the polished cross-sectioned coatings. Microhardness was measured on polished cross-sections near the central area of coatings using a Vickers tester (BUEHLER, UK) by applying a load of 25 gf for 30 s in 5 different regions along the cross-section for each sample. The phase composition of the Bioglass coatings and powder was analysed by X-ray diffraction (XRD, D500 Siemens) with a Cu K-α radiation source (1.54 Å) and a point detector. Powder and all coatings were scanned from 20° – 70° 2θ, with a step size of 0.1° and a dwell time of 3 s. Other investigations were made by micro-Raman spectrometry (Horiba LabRAM HR Raman microscope) using a 532 nm-wavelength laser as excitation source.

2.4 Interaction with the simulated body fluid (SBF)

Immersion tests in simulated body fluid (SBF) solution were performed on Bioglass coatings using disks samples of 6 mm diameter cut from coated samples using an Ormond 5 axis water-jet cutting machine (Ormond LLC, Washington) with a 1 mm diameter nozzle, 3000 bar water pressure, abrasive feed 125 g/min and cutting feed 600 mm/min. SBF solution was prepared using the detailed procedure by mixing all the reagents in the given order (see Table 2) using a magnetic stirrer while controlling pH at 6.5 ± 0.5 and temperature at 36.5 ± 0.5^{o}C [35]. The standard method (BS ISO 23317:2014) [35] was followed to make SBF solution with an appropriate concentration of ions. The discs were immersed in a specific volume of (V_s) of SBF, such that $V_s = S_a/10$ (Sa is the surface area of samples (mm^2)) in

polyethylene vials at a constant temperature of 37^{o}C. The samples were immersed for 1, 2, 3, and 7 days and then washed with double-distilled water after extraction and allowed to dry at room temperature.

The surfaces of the immersed samples were observed by SEM Quanta-600 under low vacuum. XRD was performed on these samples to identify the phase/s formed on the samples. Also, energy-dispersive X-ray analysis (EDX) analysis were conducted to explore any compositional changes on the surfaces of Bioglass coated discs using SEM (JEOL 6490, Tokyo Japan, EDX: INCA 350, Oxford Instruments, Abingdon, UK). Raman spectroscopy was done on the participated HA film by using 785 nm laser.

3 Results

3.1 Powder Characterization

The size distribution measured by laser diffraction on the suspension is given in Fig. 1 A, indicated that the suspension used for spray featuring D_{10}= 1.7 µm, D_{50}= 2 µm and D_{90}= 10 µm. From Fig. 1B it can also be seen that feedstock before suspension preparation contained a mixture of fine and coarse particles, while the largest particle size was ~ 5 µm. The peak of the particle size distribution broadened (0.8 µm-27 µm), which suggested that the Bioglass (45S5) particles were agglomerated.

3.2 As-sprayed coating microstructure

Figure 2 shows the surface morphology of as-sprayed coatings using Bioglass 45S5 suspension deposited at different flame powers of 25kW (low power), 50kW (medium power), and 75kW (high power). The surface of the coating obtained at the low flame power contained hollow/porous sphere like structures (Fig. 2A) whilst the higher magnification image (Fig. 2D) of the same low power coating showed the surface to also contain some smaller spheres which may have formed from the impact of slower and partially re-solidified Bioglass (45S5) droplets. The surface of the coating deposited using medium (50 kW) flame power contained mostly well-flattened splats with a few round particles also observed (Fig. 2B). At higher magnification these splats appeared to be non-regular shape and of approximate 5 µm in size (Fig. 2E). Some larger pores in the top surface of this coating were also observed. The higher flame power (75 kW) coating surface showed some larger porous humps (~10µm) (Fig. 2C), which probably originated from the droplets agglomerating at the higher flame power of 75 kW. Also this surface contained some rounded particles and splats of Bioglass (45S5) (Fig. 2F). The arithmetical mean deviation of the profile (Ra) of this coating was measured to be approximately 3.0 ± 0.2 µm in comparison to the other two (i.e. 25 and 50 kW) which revealed roughness values of 2.0 ± 0.1 µm and 2.1 ± 0.1µm, respectively.

The cross-sectional images of the coatings are shown in Fig. 3. As can be seen for the low flame power of 25 kW (Fig. 3A) a thin (<10 µm) non uniform coating was obtained. The microstructure of this coating suggested that the 25 kW flame power was insufficient to melt and accelerate the particles sufficiently to develop a thicker coating. It should be noted that 25 kW is also the lower end of the spray ability of this HVOF thermal spray gun, and probably resulted in a sub-sonic flame. At medium (50 kW) and high flame power (75 kW) thicker coatings of 25 ± 1 µm thickness were deposited. These coatings were porous, with the coating achieved at the high flame power appearing to be less porous (10±1 %) than the

coating deposited at medium flame power (50 kW) which revealed porosity of 16± 2%. Although, some cracks were also observed in the medium flame power coating (see Fig. 3B and these common due to the presence of thermal stresses in the coatings. It should be noted that these cracks did not propagate to the coating-substrate interface and these defects were not observed in the coating deposited using the higher flame power. Both of the medium and high-power coatings appeared to be well-adhered to the substrate, as no cracks or delamination along the coating-substrate interface were observed. The microhardness results obtained are given in Table 3, which show an increase in values with increasing flame power deposited coatings as for 50 kW coating it was 253 ±2 HV and 270 ± 1 HV for 75 kW coating. For the coating deposited at low flame power it was not possible to measure the microhardness, due to the very low thickness of coating deposited.

In order to explore the compositional gradient, local chemical analyses were carried out and the elemental (wt. %) was examined as a function of the distance from the coating-substrate interface to the top surface of the coating. Figure 4 shows the results obtained with the corresponding SEM images, where the points on the images show the locations of EDX analysis conducted. The results showed that the Bioglass 45S5 composition varied along the thickness of the coatings after thermal spray. However, the pattern of these changes was different for all three of the coatings. Fig. 4 (A & B) show the SEM image with the corresponding EDX line scan of the coating deposited at low flame power (25kW). The Si content varied from the expected 19.3 wt. % to 25 wt. % at the coating-substrate interface. Then decreased to 23.5 wt. % at the top of the coating. Na also varied from the expected 16.4 wt. % to 11 wt. % at the interface and then increased to 15 wt. % at the top surface of the coating. Whereas the variation in Ca content observed was negligible from the expected 19 wt. % to 18 wt. %. The variation in P content was also negligible fluctuating at around 2 wt. %. There was also some Fe identified near the coating-substrate interface which originated from the metal substrate surface. For the coating obtained at medium flame power (50 kW) the compositional variations were more prominent than those observed for the lower

flame power coating (Fig. 4C & D). Figure 4D also showed that the Si coating gradient varied from approximately 25 wt. % at the coating substrate interface and then decreasing to 22 wt. % at the top surface of the coating. Whereas the Na varied from 8.5 wt. % at the interface, increasing to 17 wt. % at the top of the coating. The Ca content changes were again to be more stable, with variations observed from 22 wt.% at the interface and decreasing to 20 wt. % on the top of the coating, whilst P variations were again negligible (from 2 wt.% at the interface to 2.5 wt. % at the top surface). For the coating deposited at high flame power (75 kW) the compositional gradient profiles observed from the coating- substrate interface to the coating top surface were much smoother and consistent in comparison (Fig. 4E & F), the Si variation observed was 28 wt. % at the coating substrate interface and fluctuating around 27 wt. % till the top surface of the coating. Na content was around 2 wt. % through the whole thickness of the coating. Ca varied from 22 wt. % at the coating substrate interface to 21 wt. % at the top of the coating. P remained uniform at 2 wt. % through the whole coating thickness. Although the compositional variations in the coating obtained at high flame power showed the least variation across the coating thickness, the actual variation in composition observed in comparison to the original starting Bioglass (45S5) formulation. The EDX area scan on the top surface of the coatings is given in table 4, this analysis showed that Na reduced from 16.4 wt. % (Na present in 45S5 before spray) to 9.1, 9.6 and 5.4 wt. % respectively, with increasing flame power from 25 kW, 50 kW and 75 kW. The same trend was also seen for the P content, where the initial content of 2.2 wt. % had reduced to 1.8, 1.6, and 1.2 wt. % with increasing flame power. However, Ca and Si contents showed the reverse trend of increased content with increasing flame power. Si increased from 23.5, 25.3 and 27.4 wt. % with the increasing flame power from 25, 50 and 75 kW. And Ca content was 19.4 wt. % in the 25 kW coating, 20.8 wt. % in 50 kW coating and 22.5 wt. % in 75 kW coating as well.

The XRD diffraction of the starting powder formulation and the three coatings at low, medium and high powers are shown in Figure 5. The broad hump appearing at 2θ of 25^{o} to 35^{o} in

the XRD pattern of the starting Bioglass powder and coatings obtained revealed the absence of any sharp peaks suggesting that they were of an amorphous nature. The only recognisable peaks which were labelled as austenite (PDF card no. 00-023-0298) and ferrite (PDF card no. 00-006-0696) were attributed to the stainless-steel substrate (Fig. 5A). The Raman spectra of the coatings were not different from that of the powder (Fig. 5B), and all were consistent with spectra reported in [24].The spectra of 50 kW and 75 kw coatings after 1000 cm^{-1} to 1100 cm^{-1} were different from that of the spectra of 45S5 powder and coating obtained at 25 kW. This difference may be due to the difference of microstructure. In all three spectra of the coatings, the bands observed at ~ 610 cm^{-1} and 1079 cm^{-1} were assigned to the stretching of Si-O-Si, whilst the band at 860 cm^{-1} was assigned to non-bridging oxygen–silica Si-2NBO which was of the same intensity for all the coatings and bulk glass, and the peak at 945 cm^{-1} was assigned to the stretching of PO_4^{-2} [25]. More over the Raman spectra of all the coatings were similar to that of the powder sample.

3.3 Interaction with SBF

After immersion the coated samples in SBF, it was observed that no precipitate had formed on any of the coatings after day 1. Furthermore, no precipitate was observed for the coating deposited at the lower (25 kW) flame power for up to 7 days immersion (Fig. 6A, D). However, the coatings obtained at medium (50 kW) and high (75 kW) flame power were uniformly covered with precipitate after three days (see Fig. 6B, C). Figure 6E and F suggest that with the increase of immersion time in SBF the dome like morphology of precipitated HA increased, which suggests further deposition of HA on 50 and 75 kW coatings. Also the precipitate deposited revealed cracks, which was suggested to be due to shrinkage when they were dried after removal from the SBF solution [9].

The XRD profiles of the coatings after immersion in SBF solution are shown in Fig. 7A, B. Hydroxyapatite (HA) was identified from peaks at 26^{o} and 32^{o} 2θ which matched pdf card no 00-001-1008. These peaks increased in intensity with immersion time (see Fig. 7b); however, no HA peak was identified for the coating deposited at low flame power even with longer immersion time of 7 days. Figures 7A and B suggest that austenite and ferrite peaks from the substrate were still recognizable in the XRD spectra. This is because that the precipitated HA film was not homogenous and cracked, which could be confirmed with SEM images (Fig. 6).

Raman spectroscopy analysis was performed on synthetic HA powder and the coating surfaces of the medium and higher power coated samples after immersion in SBF for 7 days (Fig. 8). The v_1 vibration mode of PO_4^{-3} exhibited a single band around 960 cm^{-1} for the HA powder and for the HA precipitated on the surfaces of the coatings. The v_2 domain for the HA powder also showed a peak at 432 cm^{-1} which was also observed for the precipitated HA on the coated samples. The peaks at 1046 cm^{-1} and 1078 cm^{-1} for the HA powder were assigned to the PO_4^{-3} v_3 vibration. However the peaks at 1070 cm^{-1} in the precipitated HA (on the surfaces of coatings) were assigned to v_1 mode of the carbonate group suggesting the carbonated nature of the precipitated HA [25]. The PO_4^{-3} v_4 vibration exhibits three peaks at 579, 590, and 608 cm^{-1}, in which 590 cm^{-1} is the strongest among these. These peaks were identified in all spectra, for the HA powder and the precipitated HA on the Bioglass (45S5) coatings[26][27].

Fig. 9 B and D are the EDX line scans along the cross-section of the medium and high flame power coatings after 7 days of immersion in SBF. Fig. 9A & C are the corresponding images of the analysed areas. Fig. 9A shows SEM image of the cross-section of the coating obtained at medium flame power after 7 days of immersion in SBF and shows that the precipitated HA layer thickness was approximately 28 µm with almost 8 µm thick residual glass underneath of this HA layer. Fig. 9B shows that Si content had reduced to 10 wt. %, which further decreased when going from the substrate- coating interface to the top surface

HA layer. However, Ca and P wt. % had increased to approximately 28 wt.% and 17 wt. %, which further increased to 37 wt. % and 20 wt. % while going from the substrate–coating interface to the top surface to the top surface of deposited HA layer.

Fig. 9C shows the cross-sectional SEM image of high flame power coating soaked in SBF for 7 days, highlighting an approximate 10 µm HA layer had been precipitated on the surface of the coating while the residual glass layer was 22 µm thick. The EDX line scan (Fig. 9D) of this coating showed that the Si content was 40 wt. % at the substrate-coating interface, then increased to approximately 43 wt. % at the interface between coating and deposited HA layer. After which a significant decrease in Si content was observed. Ca content was 5 wt. % at the coating-substrate interface and then increased to approximately 35 wt. % on top surface of HA layer. The P content showed similar profile, initially at 2 wt. % at the interface between coating and substrate and the increased to 22 wt. %.

The EDX area analysis was also conducted for the top surfaces of samples immersed for 3 and 7 days and the results are tabulated in Table 4. This analysis suggested that for 25 kW coating Si content reduced to approximately 3.7 wt. %, Ca reduced to 12.4 wt. %, Na reduced to 1.8 wt. % and P increased to 9 wt. %, also Fe increased to 9.1 wt.% and also had Cr 7.4 wt. % after immersion in SBF for 7 days. For 50 kW coating, Si content reduced to approximately 0.3 wt. %, Ca increased to 39.5 wt. %, Na reduced to 0.9 wt. % and P increased to 18.6 wt. %, after immersion in SBF for 7 days. For coating obtained at 75 kW, Si content reduced to 2.5 wt. %, Ca increased to 34.8 wt. %, Na reduced to 1.2 wt. % and P increased to 18.7 wt. %, after immersion in SBF for 7 days.

Table. 5 shows the Ca / P ratio (atomic) for all coatings before SBF testing and after immersion in SBF for 3 and 7 days. This data suggested that Ca/P ratio had decreased after 7 days immersion in SBF. After 3 days of immersion the top surfaces of coatings deposited at medium and high flame power with precipitated HA the Ca/P ratio was approximately 1.5. And with further immersion time to 7 days this ratio was 1.53 for medium flame power coating, while for high flame power it was 1.63.

4 Discussion

4.1 Microstructure formation in 45S5 coating

It was observed that increasing the flame power had a significant effect on the coating microstructure. At lower flame power of 25 kW a thin (<10 µm thickness) coating was obtained whilst at flame powers of 50 and 75 kW thicker coatings (25 ± 1 µm) were produced, with different microstructures. From these results and other literature studies based on SHVOF thermal spray, it is proposed that the lower flame power (25 kW) does not provide sufficient energy to melt and accelerate the particles to deposit onto a substrate. When these unmelted large particles and agglomerates collide onto the substrate they bounce off, impairing the deposition. The flame is regarded as being subsonic at 25 kW with a maximum temperature (2,727^{o}C) and velocity of (1,000 m/s), according to modelling work done in-house using a CFD software Fluent (not shown here). Whilst some of the molten / partially molten particles may adhere to the substrate, the low velocity does not produce a well-bonded splat, which result in formation of porous microstructure. At 50 kW 75 kW well-adhered, thick and less porous coatings with rough surfaces were obtained. The higher flame power coating was less porous than the medium flame power, which may be due to the more heat transfer form flame to the particles and melting them well resulting a denser microstrucutre [23] [28].

The roughness (Ra) of the coating surfaces increased with increasing flame power. For flame power of 75 kW coating of 3.0 ± 0.2 µm were obtained which was higher than for the coatings obtained at 25 and 50 kW flame power (2.00± 0.01 µm). The high flame power (75 kW) resulted in fully molten splats with humps on the surface which formed due to the agglomeration of molten particles in the flame which lead to the formation of large humps on the surface making it rougher [23]. Formation of humps in SHVOF sprayed coatings with alumina, titania and zirconia has been reported in detail before [29]. Similarly, microhardness values of the high flame power coating (270 ± 0.9 HV) was higher than that of the medium

power coating (253 ± 1.9 HV) which was also due to better melting of particles and agglomerates at this flame power—resulting in a denser coating. However, these values achieved were less than the microhardness of the bulk glass (586 HV) [1], and approximately similar to that reported by Bolelli et al. (296 HV for the lowest thickness of the coating which was 41± 3) for Bioglass (45S5) glass coatings obtained using SHVOF thermal spray [9].

EDX analysis of the coatings along the cross-section (Fig. 4 B, D, and F) showed that the Na_2O-CaO-SiO_2-P_2O_5 composition with respect to the initial bulk glass formulation of 45S5 had been altered due to thermal spraying. However, these changes were less in the coatings obtained at low and medium flame power than for the coatings obtained at the higher flame power. This was probably due to the higher heat transfer to the glass at high flame power and hence degradation of the feedstock powder [21]. Also, Table 4 showed a decreasing trend in wt. % of Na and P content when deposited at low, medium and high flame power; however, Si and Ca wt. % showed increasing levels with increasing flame power, which is probably due to the evaporation of volatile components from the molten glass particles at high temperature. This might be the direct evaporation of the volatile component such as P_2O_5 from the glass. Also glass components such as Na_2O evaporates from the glass in the form of NaOH after reacting with water vapours, which are present as a result of the combustion reaction [30].

The XRD spectra revealed that all 45S5 coatings were amorphous (Fig. 5A), while the three crystalline peaks observed were related to the substrate as the x-ray penetration depth for 45S5 Bioglass is 40.8 µm. The thickness of the coatings is less than the penetration depth of x-ray for Bioglass (45S5), that is why there were substrate peaks present in the XRD spectra of the coatings. The glass did not undergo crystallisation during thermal spray, which is due to the rapid heating and cooling of the feedstock , and not having enough time for crystallisation to occur [9]. Also, the Raman spectra for the surface 45S5 coatings (Fig. 5B) are similar to that of the starting 45S5 powder. However, there were slight shifts in the peaks of Si-O-Si from 1079 to 1075 cm^{-1} in the coatings obtained at 50 and 75 kW flame power but

still it can be assigned to the stretching of Si-O-Si bond. Similarly the peak at 610 cm^{-1} had shifted to 600 cm^{-1} for the coating of high flame power which was also assigned to Si-O-Si as these peaks are quite strong which is a clear indication that there is no degradation of the glass network of SHVOF deposited 45S5 coatings [9][17].

4.2 Interaction of 45S5 coating with SBF solution

The reaction mechanism of 45S5 Bioglass with SBF as reported in literature [1][31][2][32] is : (i) rapid exchange of alkali and alkaline earth ions with H^+ and H_3O^+ ions from the solution, (ii) soluble silica losses in the Si(OH) and Si-OH forms, (iii) condensation and re-polymerization of a silica rich layer, (iv) migration of Ca^{2+} and PO^{4+} to the surface and formation of an amorphous $CaO–P_2O_5$ rich film. This amorphous layer which also incorporates OH^-, $(CO_3)^{2-}$ and F^- ions from the solution crystallises into carbonated hydroxyapatite which first nucleates and then grows causing a dome- like morphology. Based on the reactions between Bioglass (45S5) and SBF all three SHVOF thermal sprayed 45S5 coatings showed different interaction with SBF. Because no HA precipitated on 25 kW coating, thick HA layer (~ 24µm) on the surface of 50 kW coating and thin HA layer (~ 17 µm) precipitated on 75 kW coating.

For the coating deposited at lower flame power of 25 kW no HA had formed even after three and seven days of immersion in SBF solution. From table 4, This suggested that the microstructure of the 25 kW coating was not stable enough for the precipitation of HA to occur on its surface [15]. Furthermore, the increasing Fe and Cr contents (from substrate) observed from this sample after immersion in SBF for 3 and 7 days, suggest that the low flame power coating may have degraded, leading to a reduction in the thickness of the coating [15].

The XRD profiles for the coatings deposited at 50 and 75 kW after immersion in SBF revealed peaks for HA (see Fig. 7A & B). The broad diffraction peak at ~32° 2θ may be due

to crystalline structural defects for example the presence of carbonated hydroxyapatite. The presence of a carbonated group is common for Bioglasses reacting with SBF for longer durations, and this group can cause the broadening of XRD peak [9].

The Ca/P ratios of the HA deposited were equal to 1.5 for the medium (50 kW) flame power coating and 1.63 for higher (75 kW) flame power coating after immersion in SBF for 7 days. Ca/P ratio equal to 1.5 is for tri calcium phosphate (TCP) which is precursor for HA [33]. However, the Ca/P ratio equal to 1.63 is slightly different from the Ca/P ratio for synthetic HA which is 1.67 [34]. The different Ca/P ratios obtained were probably due to the fact that the HA layer deposited on the after immersion in SBF was HCA rather than HA.

However, the EDX line scans along the cross-section of the coatings at 50 kW and 75 kW after immersion in SBF for 7 days (Fig. 9B & D) showed that the interaction of these two coatings with SBF was different. The differences observed in these coatings were the HA layer thickness on their surfaces, reduction in the coatings thickness and also changes in the contents of coatings after immersion in SBF for 7 days. After immersion in SBF for 7 days a thick precipitated HA layer (approximately 24 µm) was observed on the surface of the 50 kW coating, which then showed a reduction in coating thickness (from 25 µm to 6 µm) (Fig. 9A). This reduction is suggested to be due to degradation of the coating, most likely owing to the high porosity observed in that coating, resulting in larger active surface area for the ion leaching process [25]. The more porous microstructure may have also enabled infiltration of Ca and P ions from the SBF solution into the coating, as increasing levels of Ca and P were observed in this coating (see Fig. 9B).

However, 75 kW coating after immersion in SBF for 7 days (see Fig. 9D) it was observed that the Si wt. % was high in the residual glass coating and was increasing till the coating-HA layer. Then Si wt. % decreased going from the coating-HA interface to the top of the HA layer. And also Ca and P wt. % increased from the coating-HA interface to the top of the HA layer. This suggests that no Ca and P penetrated in the coating which is due to the dense microstructure of coating. Furthermore, only a small reduction in coating thickness (from 25

µm to approximately 23 µm) was observed for the higher flame power coating after immersion in SBF for 7 days with the of formation of a thinner (~ 17 µm) precipitated HA layer on its surface. These observations suggested that the coating obtained at higher 75 kW flame power followed the same reaction steps suggested in the literature for the formation of HCA precipitated on top of the residual glass coating while immersed in SBF [9][15][19].

The results suggest that the 75 kW coating provided a more stable and durable coating which could provide prolonged interaction with bone tissue. Furthermore, if more porous structures were desired, then a combination of the 50kW and 75 kW could be considered to be applied'.

5 Conclusions

The Bioglass (45S5) suspension was prepared by dispersing powder into water + IPA and the suspension was successfully deposited using SHVOF thermal spray on stainless steel substrates. The as-sprayed coatings have been studied for microstructure characterisation and phase identification, while the SBF tests were carried out to study the reactivity of these coatings. From these observations following conclusion can be drawn:

- The results suggest that SHVOF thermal spray is a viable processing technique to produce bioactive coatings, but the process parameters require careful optimisation to obtain a coating with desired thickness and porosity on the substrate.
- Thick, uniform and well-adherent coatings were obtained at 50 and 75 kW flame power with different microstructures--the coating obtained at 50 kW was more

porous while the coating at 75 kW had a higher surface roughness due to particle agglomeration.

- The feedstock did not undergo any crystallisation during the thermal spray as confirmed by the amorphous XRD spectra. The Raman spectra of the coatings were analogous to the spectrum of 45S5 feedstock powder before spray.
- The SBF results showed that no HA was precipitated on the coating deposited at 25 kW, while HA had precipitated on coatings deposited at 50 and 75 kW. However, the coating obtained at 50 kW was more porous which lead to resorbtion of the coating microstructure.
- The coating deposited at high flame power of 75 kW developed HA layer on the surface and the coating showed little degradation during immersion ion SBF.
- These observations suggest that by controlling spray parameters different microstructures were obtained which resulted in different degradation behaviour in SBF solution.

Acknowledgment:

Saira Bano acknowledges a fully funded Faculty of Engineering Research Excellence PhD scholarship for International students. We also acknowledge support from Mr. Rory Screaton for operating the thermal spray experiments, and NMRC staff and Dr. Federico Venturi for editorial support.

References

[1] M. D. O'Donnell, "Melt-Derived Bioactive Glass," *Bio-Glasses an Introd.*, pp. 13–27, 2012.
[2] L. L. Hench, "Bioceramics," *Stress Int. J. Biol. Stress*, vol. 28, pp. 1705–1728, 1998.
[3] L. L. Hench and H. A. Paschall, "Direct chemical bond of bioactive glass-ceramic materials to bone and muscle," *J. Biomed. Mater. Res.*, vol. 7, no. 3, pp. 25–42, 1973.
[4] A. Hoppe ., "In vitro cell response to Co-containing 1393 bioactive glass," *Mater. Sci.*

Eng. C, vol. 57, pp. 157–163, 2015.

[5] I. D. Xynos, M. V. J. Hukkanen, J. J. Batten, L. D. Buttery, L. L. Hench, and J. M. Polak, "Bioglass ®45S5 stimulates osteoblast turnover and enhances bone formation in vitro: Implications and applications for bone tissue engineering," *Calcif. Tissue Int.*, vol. 67, no. 4, pp. 321–329, 2000.

[6] C. Vitale-Brovarone, F. Baino, F. Tallia, C. Gervasio, and E. Verne, "Bioactive glass-derived trabecular coating: A smart solution for enhancing osteointegration of prosthetic elements," *J. Mater. Sci. Mater. Med.*, vol. 23, no. 10, pp. 2369–2380, 2012.

[7] J. Wiley, "Silicon biochemistr y," 1986.

[8] I. D. Thompson and L. L. Hcnch, "Mechanical properties of bioactive glasses, glass-ceramics and composites," *Proc. Inst. Mech. Eng. Part H J. Eng. Med.*, vol. 212, no. 2, pp. 127–136, 1998.

[9] L. Altomare ., "Microstructure and in vitro behaviour of 45S5 bioglass coatings deposited by high velocity suspension flame spraying (HVSFS)," *J. Mater. Sci. Mater. Med.*, vol. 22, no. 5, pp. 1303–1319, 2011.

[10] E. Saiz, S. Fujino, T. Oku, and K. Suganuma, "Bioactive glass coatings for orthpedic metallic implants."

[11] A. Cattini ., "Suspension plasma sprayed bioactive glass coatings: Effects of processing on microstructure, mechanical properties and in-vitro behaviour," *Surf. Coatings Technol.*, vol. 220, pp. 52–59, 2013.

[12] F. Baino and C. Vitale-Brovarone, "Feasibility of glass-ceramic coatings on alumina prosthetic implants by airbrush spraying method," *Ceram. Int.*, vol. 41, no. 2, pp. 2150–2159, 2015.

[13] G. Bolelli, V. Cannillo, R. Gadow, A. Killinger, L. Lusvarghi, and J. Rauch, "Processing and characterisation of high-velocity suspension flame sprayed (HVSFS) bioactive glass coatings," *Ceram. - Silikaty*, vol. 54, no. 1, pp. 1–7, 2010.

[14] F. Baino and E. Verne, "Glass-based coatings on biomedical implants: a state-of-the-art review," *Biomed. Glas.*, vol. 3, no. 1, pp. 1–17, 2017.

[15] J. P. Borrajo , "The role of the thickness and the substrate on the in vitro bioactivity of silica-based glass coatings," *Mater. Sci. Eng. C*, vol. 25, no. 2, pp. 187–193, 2005.

[16] A. K. b Giovanni Bolelli a,∗, Johannes Rauch b, Valeria Cannillo a and R. G. Luca Lusvarghi a, "Investigation of High-Velocity Suspension Flame Sprayed (HVSFS) glass coatings," *Mater. Lett.*, vol. 62, pp. 2772–2775, 2008.

[17] G. Bolelli, V. Cannillo, R. Gadow, A. Killinger, L. Lusvarghi, and J. Rauch, "Processing and characterisation of high-velocity suspension flame sprayed (HVSFS) bioactive glass coatings," *Ceram. - Silikaty*, vol. 54, no. 1, pp. 1–7, 2010.

[18] N. Stiegler ., "High-velocity suspension flame sprayed (HVSFS) hydroxyapatite coatings for biomedical applications," *J. Therm. Spray Technol.*, vol. 21, no. 2, pp. 275–287, 2012.

[19] G. Bolelli ., "Comparison between Suspension Plasma Sprayed and High Velocity Suspension Flame Sprayed bioactive coatings," *Surf. Coatings Technol.*, vol. 280, pp. 232–249, 2015.

[20] G. Bolelli ., "Suspension thermal spraying of hydroxyapatite: Microstructure and in vitro behaviour," *Mater. Sci. Eng. C*, vol. 34, no. 1, pp. 287–303, 2014.

[21] R. Moreno, "The role of Slip additives in tape casting technology: Solvents and dispersants," *Am. Ceram. Soc.*, vol. 71, pp. 1521–1531, 1992.

[22] S. Cabanas-Polo and A. R. Boccaccini, "Understanding Bioactive Glass Powder Suspensions for Electrophoretic Deposition of Bioactive Glass-Polymer Coatings," *J. Electrochem. Soc.*, vol. 162, no. 11, pp. D3077–D3083, 2015.

[23] M. Bai, R. Khammas, L. Guan, J. W. Murray, and T. Hussain, "Suspension high

velocity oxy-fuel spraying of a rutile TiO2feedstock: Microstructure, phase evolution and photocatalytic behaviour," *Ceram. Int.*, vol. 43, no. 17, pp. 15288–15295, 2017.

[24] D. Bellucci, G. Bolelli, V. Cannillo, A. Cattini, and A. Sola, "In situ Raman spectroscopy investigation of bioactive glass reactivity: Simulated body fluid solution vs TRIS-buffered solution," *Mater. Charact.*, vol. 62, no. 10, pp. 1021–1028, 2011.

[25] A. Hoppe., "In vitro reactivity of Cu doped 45S5 Bioglass derived scaffolds for bone tissue engineering," *J. Mater. Chem. B*, vol. 1, no. 41, pp. 5659–5674, 2013.

[26] R. Cuscó, F. Guitián, S. de Aza, L. Artús, S. de Aza, and L. Artús, "Differentiation between hydroxyapatite and β-tricalcium phosphate by means of μ-Raman spectroscopy," *J. Eur. Ceram. Soc.*, vol. 18, no. 9, pp. 1301–1305, 1998.

[27] G. Penel, G. Leroy, C. Rey, and E. Bres, "MicroRaman Spectral Study of the PO 4 and CO 3 Vibrational Modes in Synthetic and Biological Apatites," *Calcif. Tissue Int.*, vol. 63, no. 6, pp. 475–481, 1998.

[28] Z. Pala, E. Shaw, J. W. Murray, N. Senin, and T. Hussain, "Suspension high velocity oxy-fuel spraying of TiO2: A quantitative approach to phase composition," *J. Eur. Ceram. Soc.*, vol. 37, no. 2, pp. 801–810, 2017.

[29] M. Bai, H. Maher, Z. Pala, and T. Hussain, "Microstructure and phase stability of suspension high velocity oxy-fuel sprayed yttria stabilised zirconia coatings from aqueous and ethanol based suspensions," *J. Eur. Ceram. Soc.*, vol. 38, no. 4, pp. 1878–1887, 2018.

[30] R. G. C. Beerkens, "Modeling the kinetics of volatilization from glass melts," *J. Am. Ceram. Soc.*, vol. 84, no. 9, pp. 1952–1960, 2001.

[31] W. Cao and L. L. Hench, "Bioactive materials," *Ceram. Int.*, vol. 22, no. 6, pp. 493–507, 1996.

[32] L. L. Hench, "Bioceramics: From Concept to Clinic," *J. Am. Ceram. Soc.*, vol. 74, no. 7, pp. 1487–1510, 1991.

[33] M. Ebrahimi, M. G. Botelho, and S. V. Dorozhkin, "Biphasic calcium phosphates bioceramics (HA/TCP): Concept, physicochemical properties and the impact of standardization of study protocols in biomaterials research," *Mater. Sci. Eng. C*, vol. 71, pp. 1293–1312, 2017.

[34] M. T. Islam, K. M. Z. Hossain, N. Sharmin, A. J. Parsons, and I. Ahmed, "Effect of magnesium content on bioactivity of near invert phosphate-based glasses," *Int. J. Appl. Glas. Sci.*, vol. 8, no. 4, pp. 391–402, 2017.

[35] BS ISO 23317:2014 - Implants for surgery - In vitro evaluation for apatite-forming ability of implant materials

Figure 1: (A) Feedstock particle size distribution and (B) secondary electron SEM image of ball-milled Bioglass (45S5) powder.

Figure 2: SEM SE images showing the surface morphology of the coatings deposited at different flame power: 25 kW (A and D), 50 kW (B and E), and 75 kW (C and F). The top row shows low magnification SE images and the bottom row shows high magnification images of the same area.

Figure 3: BSE SEM cross-section images showing the microstructure of the coatings deposited at different flame power: 25 kW (A), 50 kW (B), and 75 kW (C).

Figure 4: SEM SE images of the cross-section of coatings deposited at 25 kW (A), 50 kW (C), and 75 kW (E) and their respective EDX line scans through the coating cross-section in B, D and F. Points in the SEM images show the location of EDX data points in the graph.

Figure 5: XRD spectra (A) and Raman spectra (B) developed on the surfaces of the S-HVOF deposited bioglass coatings at different flame powers where R25 is 25kW, R50 is 50 kW and R75 is 75kW

Figure 6: SE SEM images showing the surface morphology of the coatings after 3 days soaking in SBF solution (A), (B), (C) and after 7days soaking (D), (E), (F). Images (A) and (D) at 25kW, (B) and (E) at 50kW, and (C) and (F) at 75kW flame power.

Figure 7: XRD scan (A) 45S5 coatings after 3 days of soaking in SBF solution and XRD scan 45S5 coatings after 7 days of soaking in SBF solution (B)

Figure 8: Raman spectra acquired on the surfaces of the S-HVOF thermal spray deposited bioglass coatings at flame powers of 50 kW and 75 kW after 7 days of soaking in SBF.

Figure 9: BSE SEM images of the cross-section of coatings deposited at 50 kW (A), and 75 kW (C) after soaking for 7 days in SBF and their respective EDX line scans in B and D. Points in the images show the location of the EDX points.

Table 1: Process parameters for S-HVOF spraying of Bioglass (45S5) coatings

Run. Number	H_2 flow rate (slpm)	O_2 flow rate (slpm)	Torch passes	Flame heat power (kW)
R25	182	77.9	20	25
R50	355	152	20	50
R75	527	226	20	75

Table 2: Physical and mechanical properties of 45S5 coatings (mean value ± standard error) produced from S-HVOF thermal spray

Run No.	Thickness (µm)	Porosity (%)	Microhardness (HV)	Surface Roughness (µm)
R25	10 ± 1	-	-	2.0 ± 0.1
R50	25 ± 1	16 ± 2	253 ±2	2.1 ± 0.1
R75	25 ± 1	10 ± 1	270 ± 1	3.0 ± 0.2

Table3: EDX area scan on top surfaces of the coatings before SBF tests and soaking in SBF for 3 and 7 days, while R25, R50 and R75 are low, medium and high flame powers.

Elements	**45S5 powder (wt. %)**	**As-sprayed (wt. %)**			**After soaking for 3 days in SBF (wt. %)**			**After soaking for 7 days in SBF (wt.%)**		
		R25	R50	R75	R25	R50	R75	R25	R50	R75
Si	19.3	23.5	25.3	27.4	28.6	1.2	5.4	3.7	0.3	2.5
Ca	17.7	19.4	20.8	22.5	10.1	37.0	32.9	12.4	39.5	34.8
Na	16.4	9.1	9.6	5.4	2.2	1.2	1.5	1.8	0.9	1.2
P	2.2	1.8	1.6	1.2	4.3	19.2	17.3	9.0	18.6	18.7
Fe	00	5.0	0.0	0.0	6.3	0.0	0.0	9.1	0.0	0.0
Cr	00	0.9	0.0	0.0	2	0.0	0.0	7.4	0.0	0.0

Table: 4 Ca/P ratio (atomic %) of the as sprayed and soaking in SBF after 3 and 7 days

Thermal Spray Coating at the corresponding flame power	**Ca/P ratio soaking for 0 days in SBF**	**Ca/P ratio soaking for 3 days in SBF**	**Ca/P ratio soaking for 7 days in SBF**
R25	7.6	1.8	1.04
R50	11	1.48	1.5
R75	10.4	1.47	1.63

Highlights

- Thick, uniform and well-adherent coatings were obtained at 50 and 75 kW flame power.
- Thin, non- uniform and porous coating was deposited at 25 kW flame power.
- XRD and Raman spectra showed no phase or structure change due to thermal spraying.
- 3 day SBF soaking led to HA deposition only on 50 and 75 kW coatings.
- Coating sprayed at 50 kW degraded more than 75 kW in SBF due to more porosity.

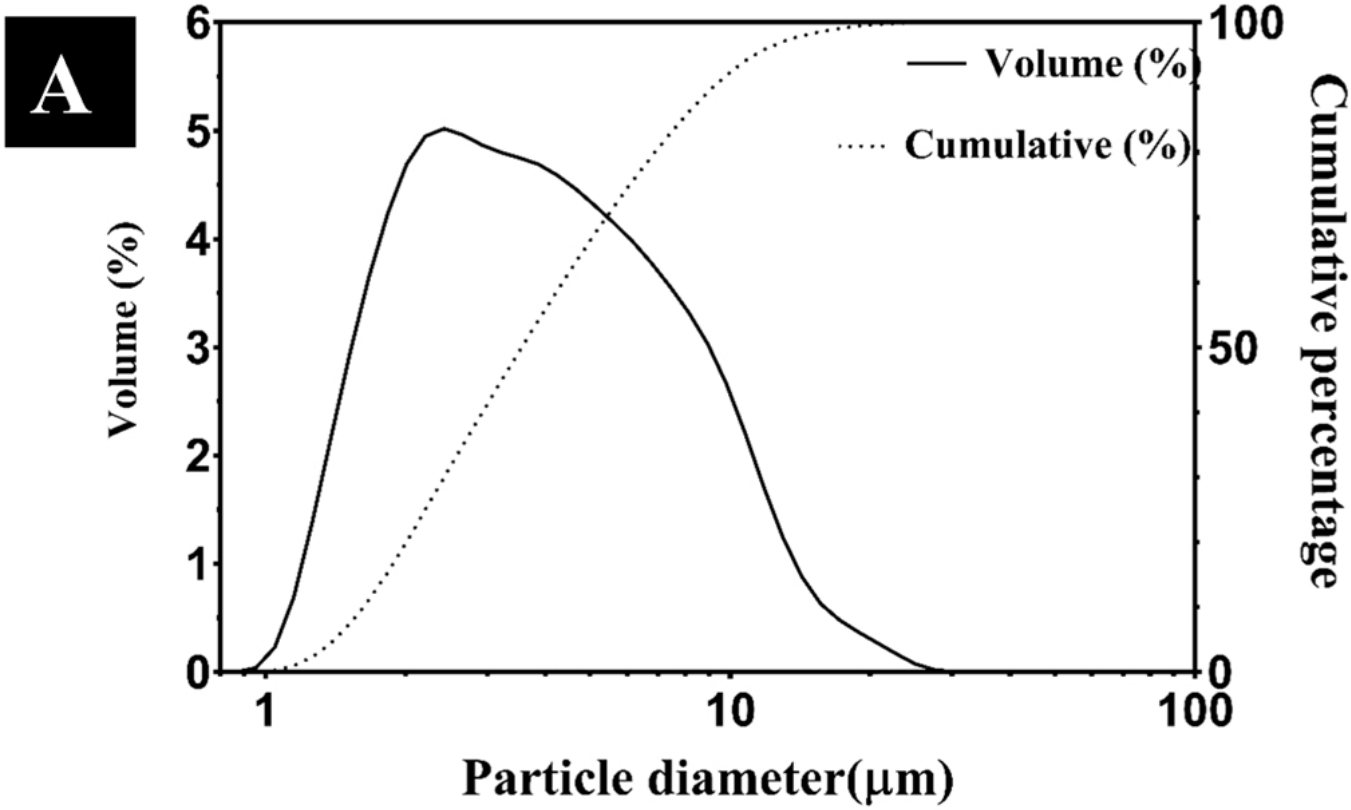
A
Volume (%)
Cumulative (%)
Volume (%)
Cumulative percentage
Particle diameter(μm)
0
1
2
3
4
5
6
50
100
1
10
100

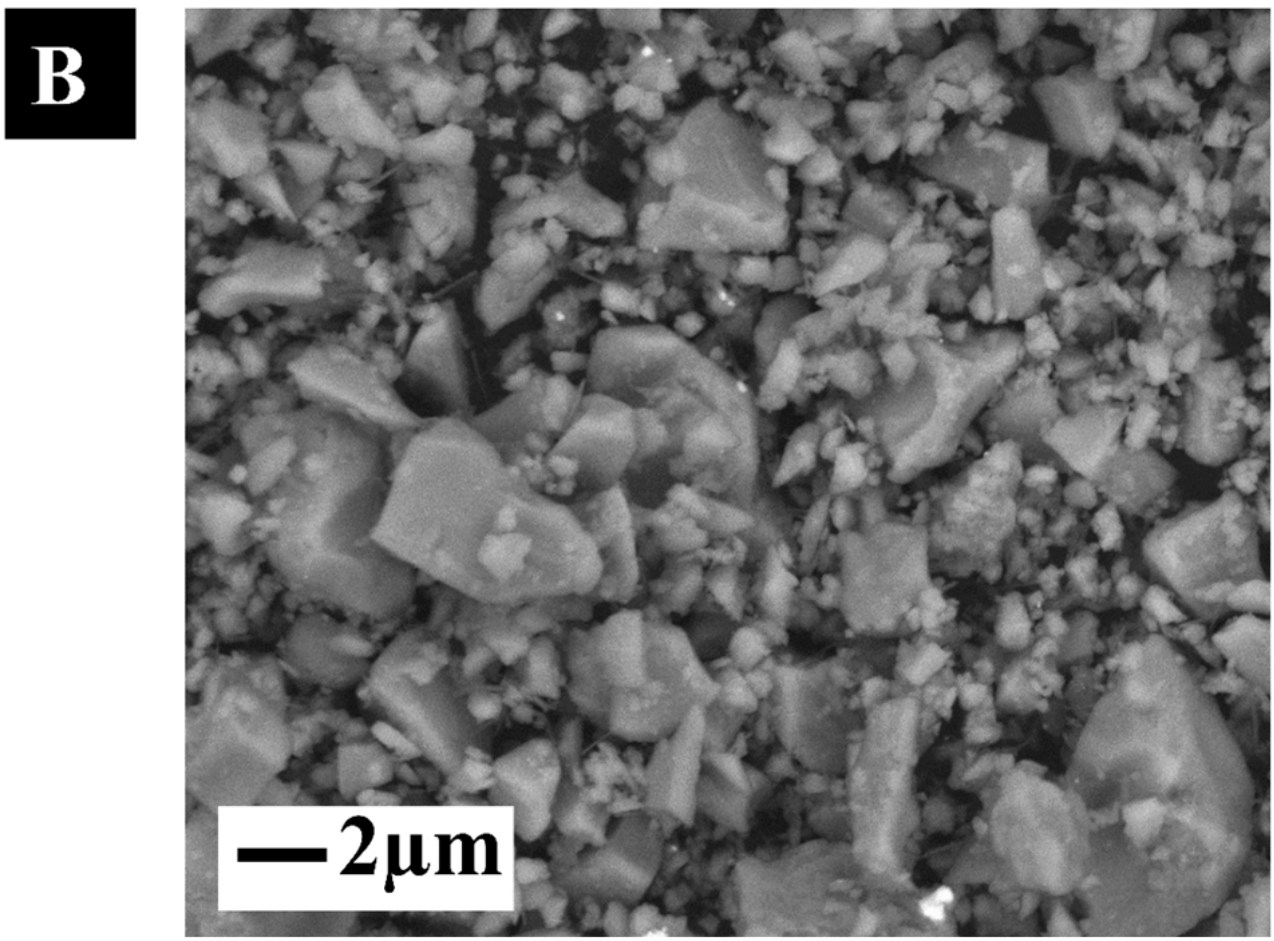
B
2μm

Figure 1

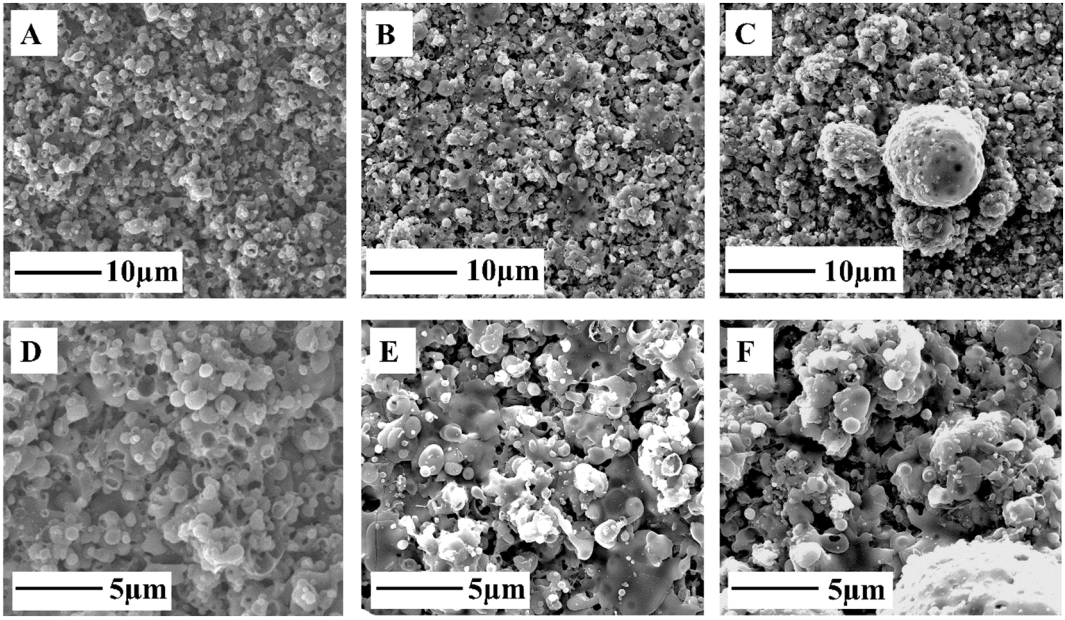

Figure 2

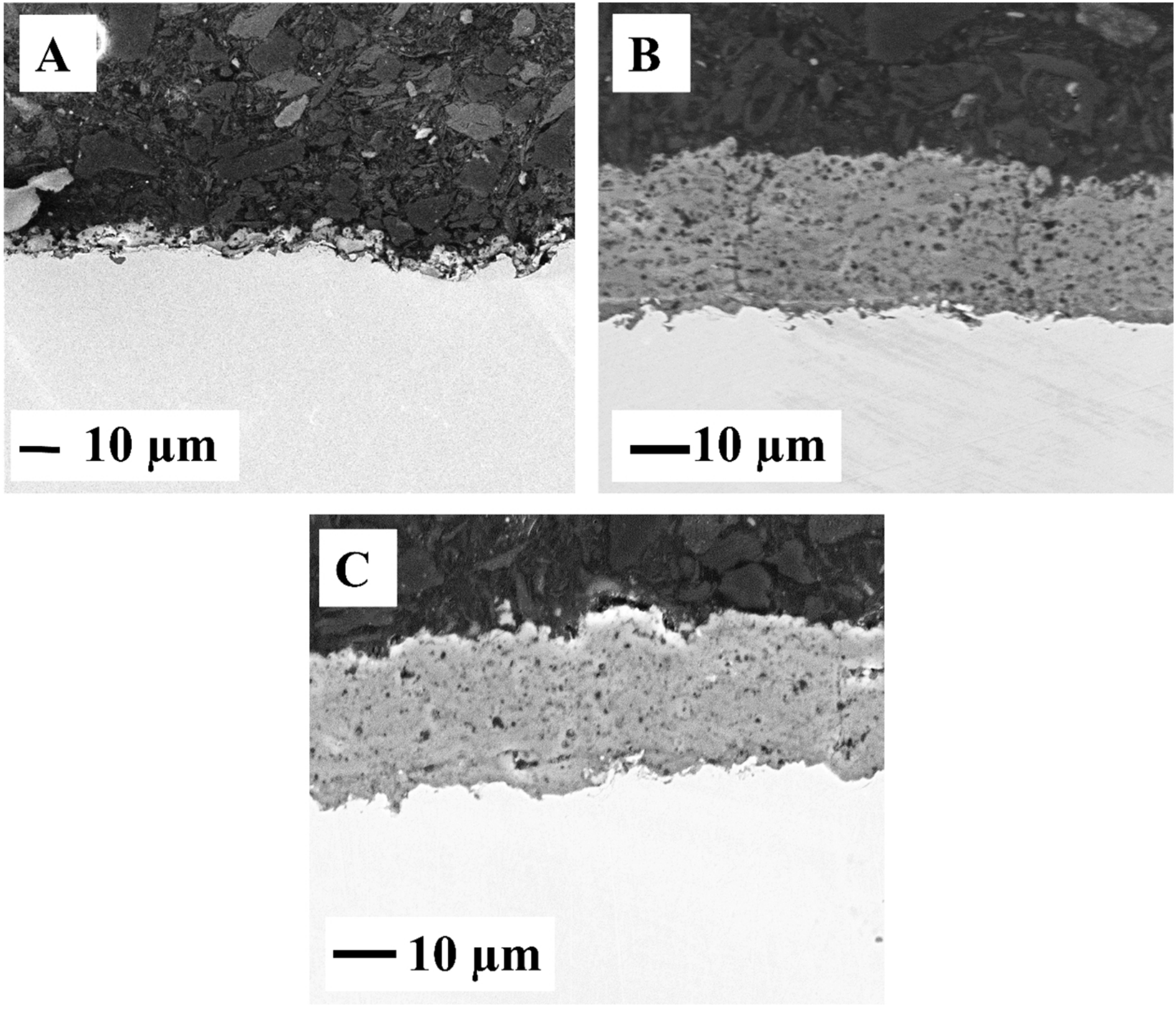

Figure 3

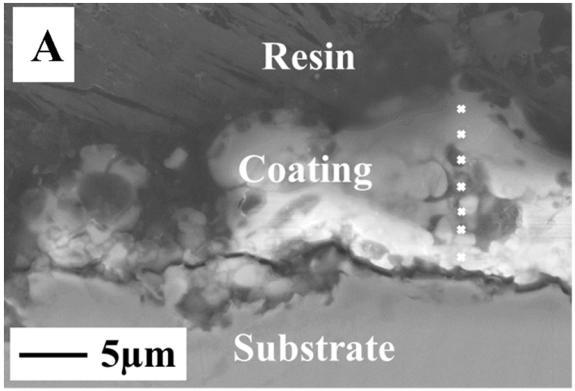
A
Resin
Coating
5µm
Substrate

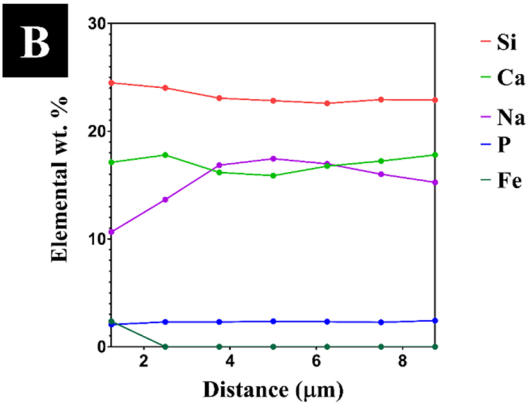
B
Elemental wt. %
Distance (µm)
Si
Ca
Na
P
Fe

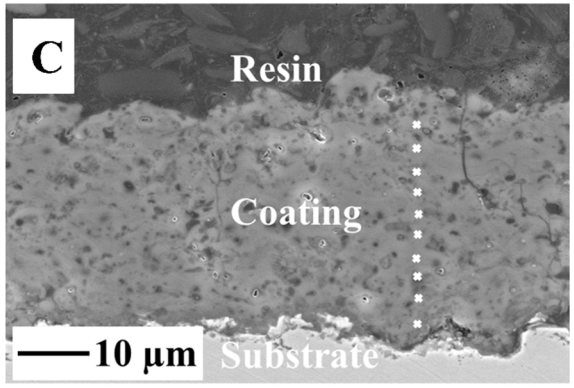
C
Resin
Coating
10 µm
Substrate

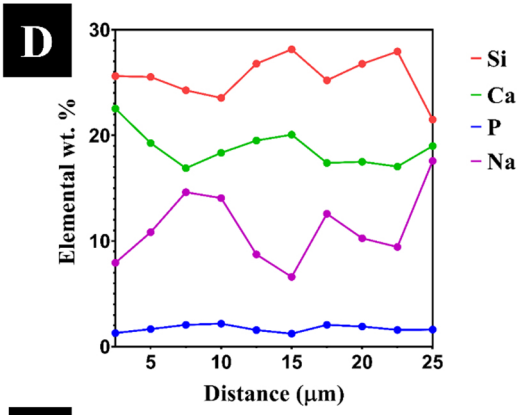
D
Elemental wt. %
Distance (µm)
Si
Ca
P
Na

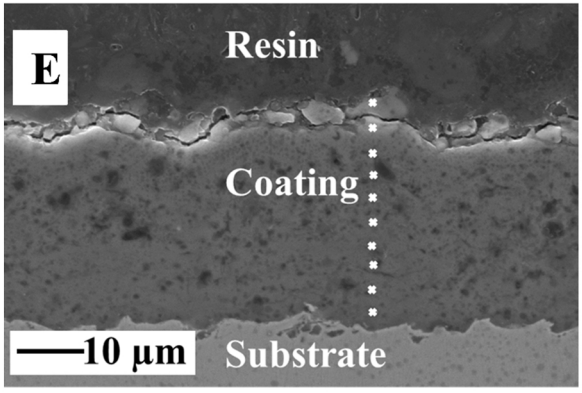
E
Resin
Coating
10 µm
Substrate

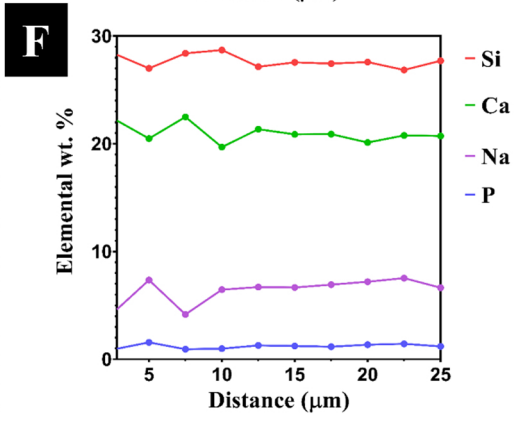
F
Elemental wt. %
Distance (µm)
Si
Ca
Na
P

Figure 4

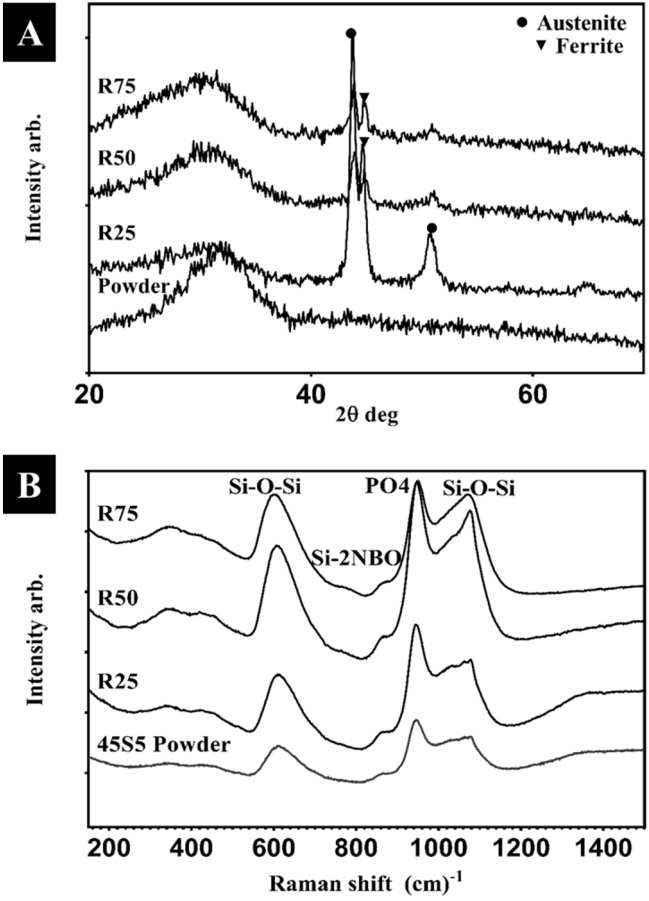
A
Austenite
Ferrite
R75
R50
R25
Powder
Intensity arb.
20
40
60
2θ deg
B
Si-O-Si
PO4
Si-O-Si
Si-2NBO
R75
R50
R25
45S5 Powder
Intensity arb.
200
400
600
800
1000
1200
1400
Raman shift (cm)-1

Figure 5

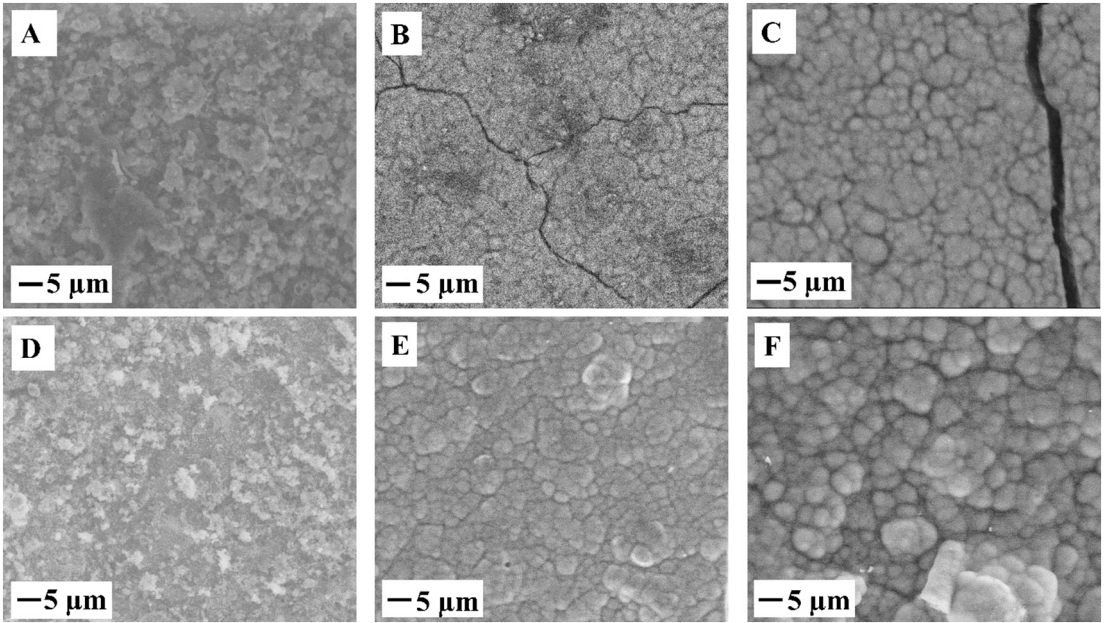

Figure 6

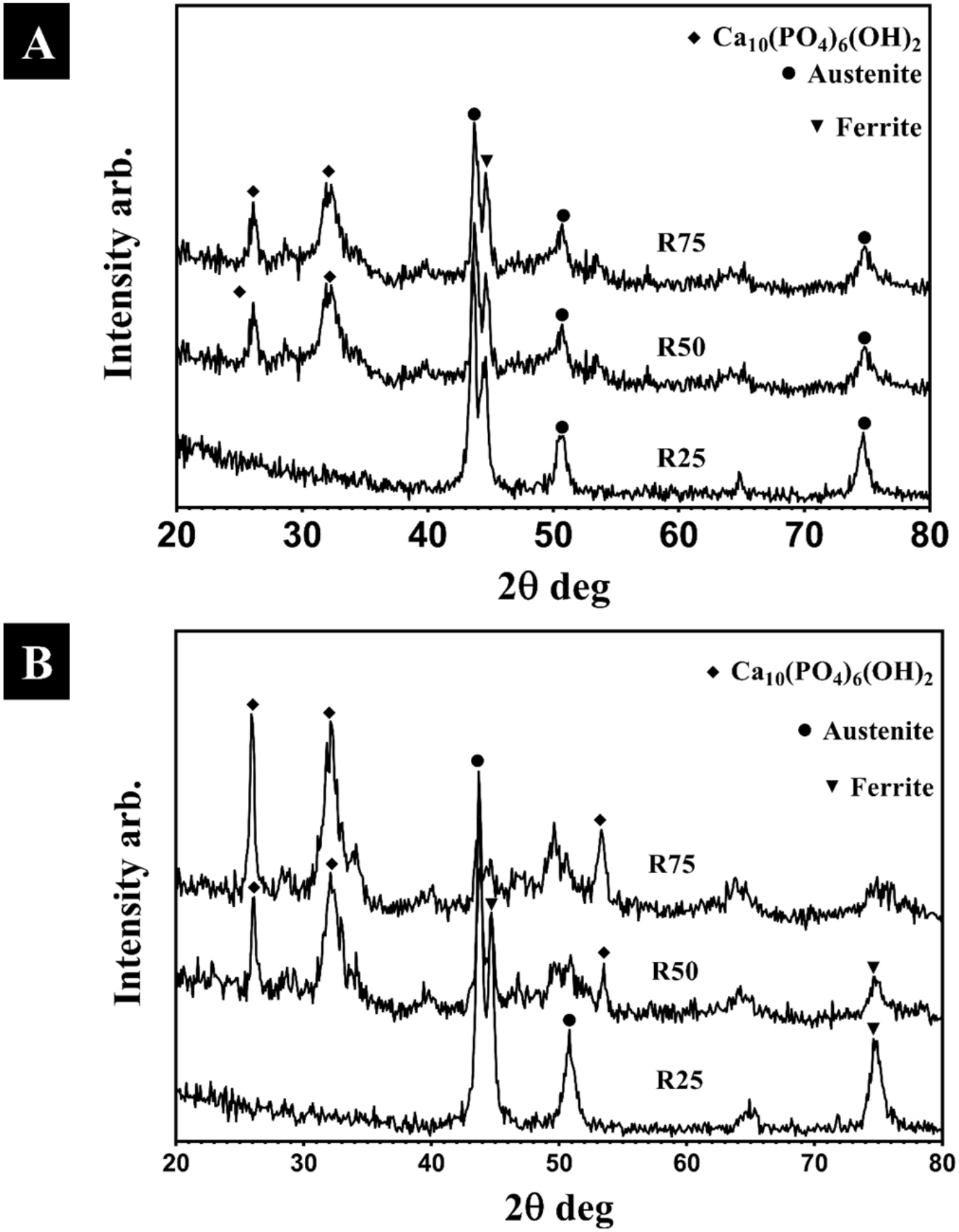
A
◆ Ca10(PO4)6(OH)2
● Austenite
▼ Ferrite
Intensity arb.
R75
R50
R25
20
30
40
50
60
70
80
2θ deg
B
◆ Ca10(PO4)6(OH)2
● Austenite
▼ Ferrite
Intensity arb.
R75
R50
R25
20
30
40
50
60
70
80
2θ deg

Figure 7

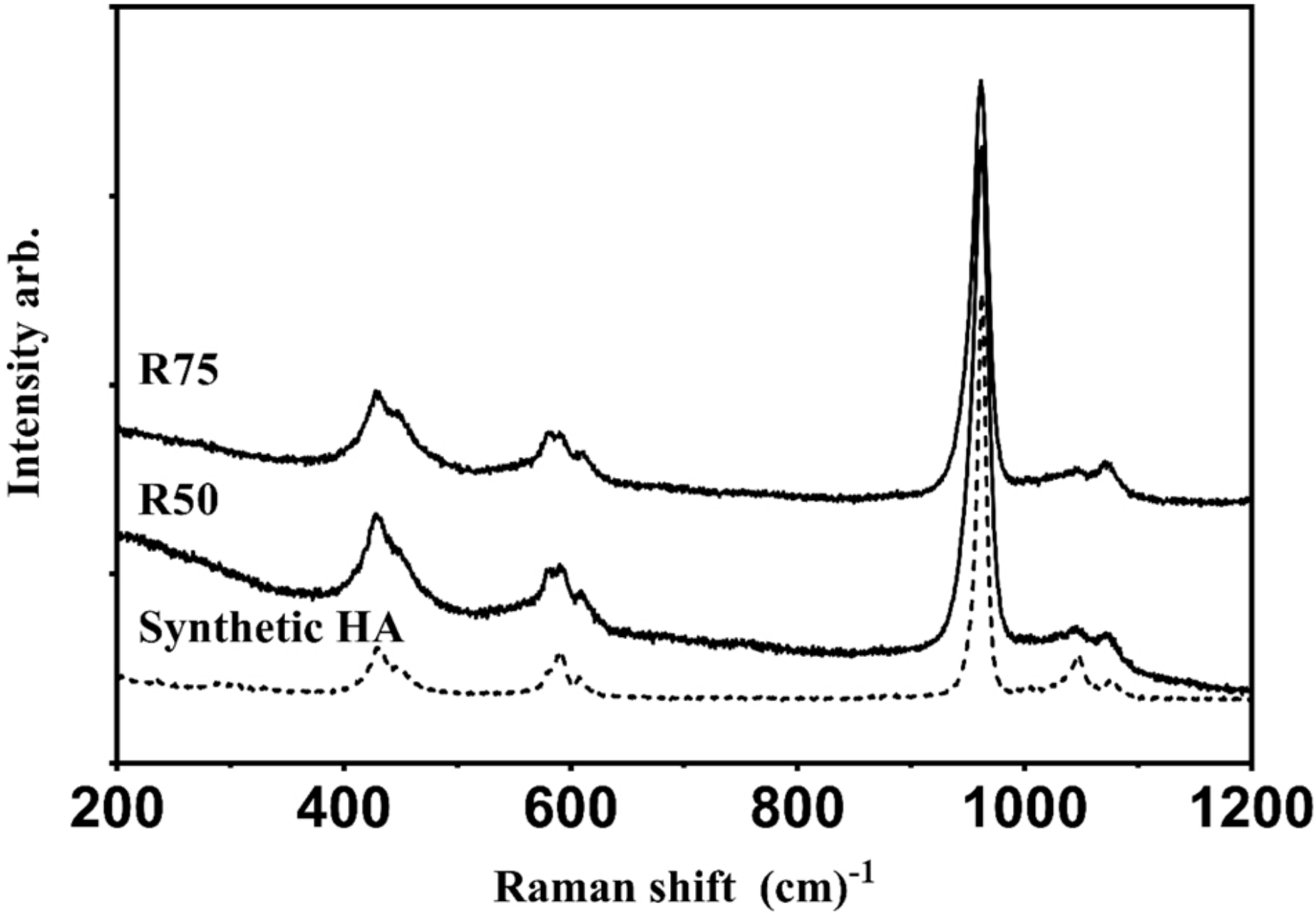
Intensity arb.
R75
R50
Synthetic HA
200
400
600
800
1000
1200
Raman shift (cm)-1

Figure 8

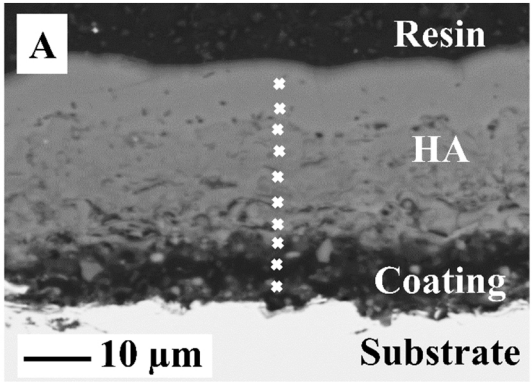
A
Resin
HA
Coating
Substrate
10 µm

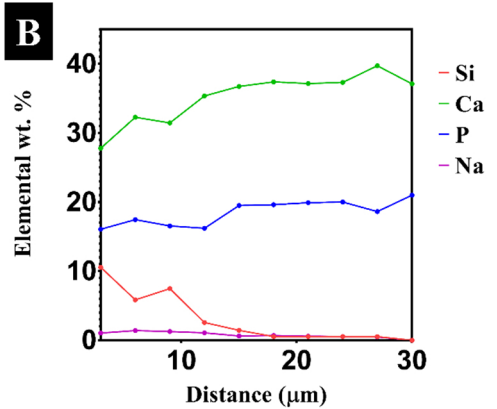
B
Elemental wt. %
Distance (µm)
Si
Ca
P
Na
0
10
20
30
40

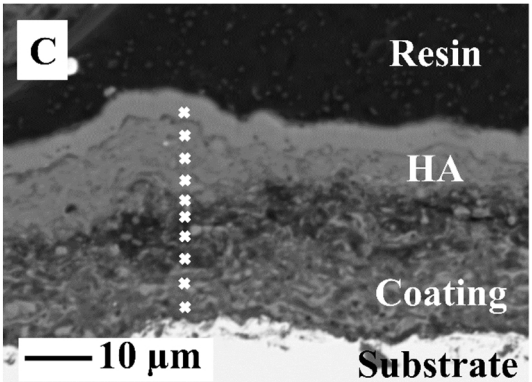
C
Resin
HA
Coating
Substrate
10 µm

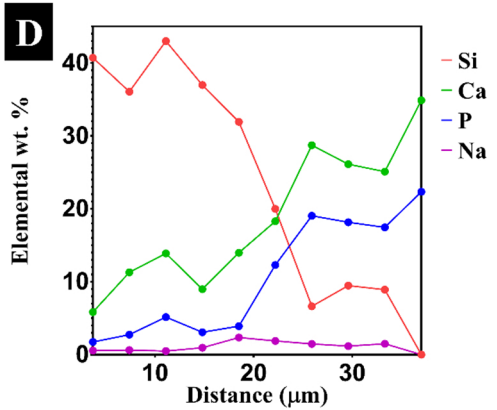
D
Elemental wt. %
Distance (µm)
Si
Ca
P
Na
0
10
20
30
40

Figure 9